

Capture CO₂ as an admixture to improve engineering performance of ultra-high performance concrete

Yi Han¹, Runsheng Lin^{1,2}, Xiao-Yong Wang^{1,2,*}

¹ Department of Integrated Energy and Infra System, Kangwon National University, Chuncheon-Si, 24341, South Korea

² Department of Architectural Engineering, Kangwon National University, Chuncheon-Si, 24341, South Korea

* Corresponding author, E-mail address: wxbrave@kangwon.ac.kr

Abstract

Ultra-high-performance concrete (UHPC) exhibits high compressive strength and good durability. However, owing to the dense microstructure of UHPC, carbonation curing cannot be performed to capture and sequester carbon dioxide (CO₂). In this study, CO₂ was added to UHPC indirectly. Gaseous CO₂ was first converted into solid calcium carbonate (CaCO₃) using calcium hydroxide, and the converted CaCO₃ was then added to UHPC at 2, 4, and 6 wt.% based on the cementitious material. The performance and sustainability of UHPC with indirect CO₂ addition were investigated through macroscopic and microscopic experiments. The experimental results showed that the method used did not negatively affect the performance of UHPC. Compared with the control group, the early strength, ultrasonic velocity, and resistivity of UHPC containing solid CO₂ improved to varying degrees. Microscopic experiments, such as heat of hydration and thermogravimetric analysis (TGA), demonstrated that adding captured CO₂ accelerated the hydration rate of the paste. Finally, the CO₂ emissions were normalized according to the compressive strength and resistivity at 28 days. The results indicated that the CO₂ emissions per unit compressive strength and unit resistivity of UHPC with CO₂ were lower than those of the control group.

Keywords: Ultra-high-performance concrete; Microstructure; CO₂ absorption.

1. Introduction

Ultra-high-performance concrete (UHPC) has a low water to cement ratio and a denser microstructure than that ordinary concrete. Therefore, its compressive strength and durability are better than that of ordinary concrete [1,2]. In addition, supplementary cementitious materials (SCMs) with pozzolanic reactivity are often added to increase concrete compressive strength and durability [3] [4] [5]. The SCMs most commonly used in UHPC has silica fume, fly ash, and blast-furnace slag [6] [7].

Because SCMs are by-products produced by other industries, adding them to concrete can provide both environmental protection and economic benefits. Isaia et al. [8] investigated the physical impacts of mineral additions and the influence of pozzolan on the performance of UHPC and found that as the concentration of mineral additives in UHPC increased, the pozzolanic and physical impacts became more significant.

Ghafari et al. [9] studied the effect of adding SCMs to the self-shrinkage properties of UHPC. The results showed that the main factor affecting the property was the total porosity of the paste. In addition, studies have found that the inclusion of blast furnace slag and fly ash increased the number of pores in the paste, leading to increased autogenous shrinkage [9].

The CO₂ concentration in the atmosphere has increased continuously since the 1860s [10][11][12]. Global temperatures rise owing to the continuous increase in CO₂, resulting in a greenhouse effect [13][14]. The Paris Agreement was signed by 175 countries to combat the impact of climate change [10]. An increasing number of researchers are working to reduce CO₂ emissions, and CO₂ capture and storage technologies have emerged in the cement concrete industry [15][16][17][18][19].

Carbonation curing of cement-based materials using CO₂ is one of the most commonly used methods. Carbon curing has many advantages and can improve the compressive strength and durability of concrete and prevent sulfate attack and chloride-ion penetration [20][21][22].

Based on the literature studies, the research gaps of previous works are summarized as follows: first, carbonation curing is only suitable for precast concrete components. For cast-in-place concrete components, the carbonation-curing method is no longer practical. Second, the current research on concrete carbonation curing is limited to thin concrete specimens; completely carbonizing large-volume concrete in a short time is challenging. Additionally, excessive carbon curing can destroy the main hydration product (CSH) inside the concrete, thereby reducing the strength of the concrete [23]. In addition, concretes that can be cured by carbonation have high water to cement ratios (approximately 0.5) [24] [25]. Owing to the dense microstructure of UHPC, the low porosity prevents CO₂ from entering the paste interior. Therefore, UHPC cannot be carbonized and solidified.

In this study, an absorbent was used to absorb CO₂ and transform gaseous CO₂ into a solid. The absorbed CO₂ was then added to a UHPC as an admixture. Calcium hydroxide (CH) was used to convert gaseous CO₂ into solid CaCO₃ (CC), which was added to UHPC at 2, 4, and 6% based on cementitious material. First, the compressive, flexural, and ultrasonic strengths and resistivity of the mortars were investigated. Second, the hydration heat of the paste was determined; its microstructure was characterized by thermogravimetric analysis (TGA), attenuated total reflectance Fourier transform infrared spectroscopy (ATR-FTIR), and X-ray diffraction (XRD). Third, the CO₂ emissions per unit volume of UHPC were calculated, and normalized according to the compressive strength and resistivity at 28 days. The following points were researched and assessed based on macroscopic and microscopic experiments: (1) the effect of CC on the macroscopic properties of the mortars in the early stage was investigated based on the heat of hydration of the paste; (2) the microstructural changes of the paste in the early and late stages were studied, and the development of the strength, ultrasonic wave, and resistivity of the mortars was analyzed combined with the microscopic analysis; (3) the UHPC sustainability was analyzed based on its compressive strength and resistivity.

The novelties and significances of this study are summarized as follows: based on the transformation of gaseous CO₂ into solid calcium carbonate, the proposed method can be used to produce both precast

concrete and cast-in-site concrete.

Moreover, because converted solid calcium carbonate is added into the mixture during the mixing process, the slow diffusion process of CO₂ from the environment to the inside of the specimen is avoided, and the proposed method is valid for high-strength concrete with low porosity. Moreover, the life cycle analysis process considers the CO₂ emission from reactants of solid calcium carbonate production.

Although abundant works have been done about blended concrete containing calcium carbonate, to the best knowledge of authors, the transformation of gaseous CO₂ into solid calcium carbonate and its utilization in UHPC has not been done.

2. Experimental

2.1 Raw materials

The CH used to prepare CC was purchased from Daejung Chemical Co., Ltd. Commercially available 100% CO₂ was used in this study. CC was prepared according to the method described by Qin et al. [26]. First, CH was dissolved in deionized water to obtain a CH solution. Second, CO₂ was fed into the CH solution at a rate of 20 L/min until the pH of the suspension reached approximately 7, and the solute of the suspension in the container was nano-CaCO₃. Third, a centrifuge was used to separate the nano-CaCO₃ suspension from liquid and solid. The collected CaCO₃ was dried at 200 °C for 24 h to evaporate the water. Finally, the dried CaCO₃ was ground into powder using an agate mortar. Gaseous CO₂ transformation into solid CaCO₃ was realized through CaCO₃ preparation. The prepared CaCO₃ was submicron. Unlike nanomaterials, submicron CaCO₃ cannot cause excessive loss of fluidity, which is convenient for engineering applications.

The microstructure of the prepared CC powders was characterized by ATR-FTIR and ultrahigh-resolution scanning electron microscopy (UHR-SEM), as shown in Figure 1. Figure 1 shows the ATR-FTIR spectrum of the CC. A pronounced CC absorption peak was found; however, the presence of CH was not detected. The CC was cubic with an average side length of approximately 300 nm, as shown in the SEM image in Figure 1b.

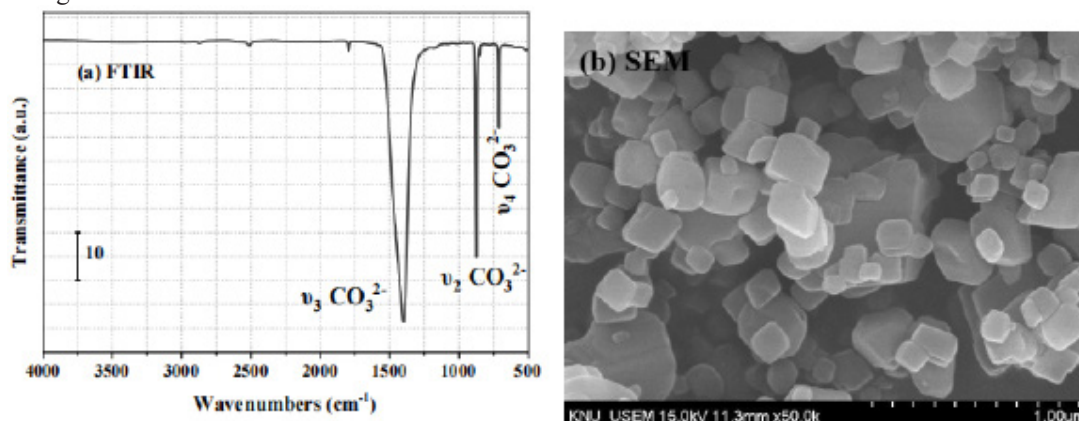


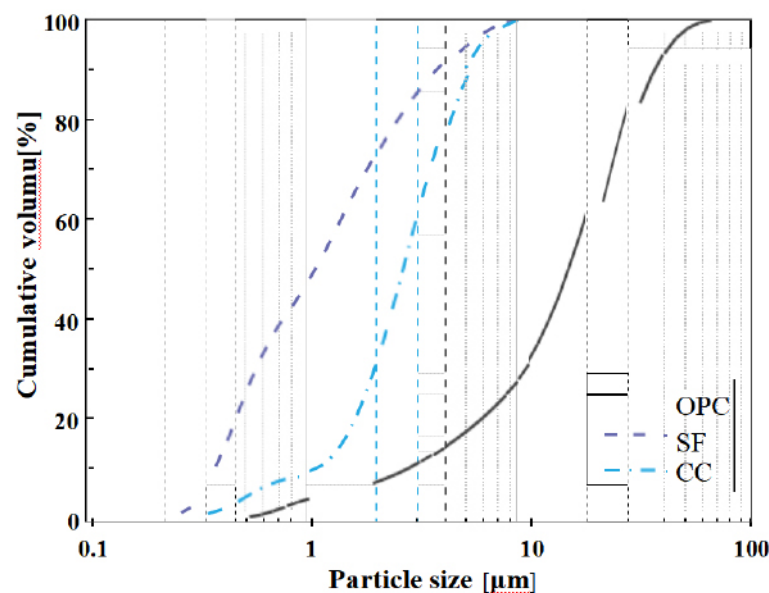
Figure 1. (a) FTIR spectra and (b) SEM of the CaCO₃ powder.

The Portland cement (OPC) used in this study was a Korean Sungshin portland cement, conforming to the Korean standard KS L 5201. The silica fume (SF) was purchased from the Korean company Boram Chemical. Table 1 shows the chemical compositions of OPC, CC, and SF from X-ray fluorescence measurements. Figure 2 shows the cumulative particle size distribution curves. The median particle sizes (d₅₀) of OPC, CC, and SF was 17.3, 2.99, and 1.23 μm, respectively.

Table 1. Chemical compositions (wt.%) of cement (OPC), silica fume (SF), and CaCO₃(CC).

	OPC	SF	CC
SiO ₂	20.70	96.00	-
Al ₂ O ₃	5.09	-	-
Fe ₂ O ₃	2.56	0.39	-
CaO	63.52	0.32	55.17
MgO	2.14	1.18	-
TiO ₂	0.26	-	-
SO ₃	2.45	0.26	-
P ₂ O ₅	0.19	0.17	-
K ₂ O	0.90	0.76	-
MnO	0.07	-	-
ZnO	0.05	0.16	-
LOI ¹	2.05	0.78	44.80

¹ Loss on ignition.

Figure 2. Cumulative volume of cement (POC), silica fume (SF), and CaCO₃ (CC).

2.2 Mix proportions

The paste and mortar samples prepared for this study are listed in Table 2. Pure paste was used for the hydration heat and microscopic characterization experiments. Mortar was used for macro tests, such as strength and non-destructive testing. The water-binder ratio (w/b) of both the paste and mortar samples was 0.2, the value widely used to prepare UHPC. The binder-mortar ratio (b/s) was 1. The mixture without CC was

used as the control (CC0). The prepared CC was added at 2, 4, and 6% of the cementitious material; the cement and silica fume contents were simultaneously reduced in proportion. In addition, the amount of superplasticizer (SP) was the same for all the mix ratios (2 %).

Table 2. Experimental mix proportions based on the binder (wt.%).

NO.	OPC	SF	CC	Water	SP	Sand
CC0	85	15	0	20	2	100
CC2	83.3	14.7	2	20	2	100
CC4	81.6	14.4	4	20	2	100
CC6	79.9	14.1	6	20	2	100

2.3 Test methods

Before the mortar and paste were mixed, the CC and water required for the experiment were first added to the container, mixed, and dispersed using ultrasonication waves. After the dispersion was complete, the mix was poured into the dry-mixed cement and silica fume. Finally, the mixture was mechanically stirred.

2.3.1 Heat of hydration

A TAM Air isothermal calorimeter was used to measure the hydration heat release rate at 20 °C for 72 hours. After the paste was mixed, 5 g of the paste was weighed into an ampoule bottle and immediately placed in the TAM Air isothermal calorimeter. Because the specific heat capacity of glass is similar to that of cement, glass was used as the specific heat capacity control material during the tests [27].

2.3.2 Mechanical properties

The compressive strength tests were performed according to the ASTM C349 standard [28]. The size of the cube mold used in the test was 50 × 50 × 50 mm³, and the test was conducted at curing ages of 3, 7, and 28 days. According to the ASTM C78 standard [29], a 40 × 40 × 160 mm³ cuboid sample is used to conduct a three-point bending test when the curing age is 28 days. Three samples were tested for each mixing ratio, and the results were averaged.

2.3.3 Non-destructive testing

Ultrasonic testing was performed using a portable non-destructive digital indicator produced by the Swiss company Proceq. Longitudinal P-wave velocity tests were performed according to ASTM C597 [30] at curing ages of 3, 7, and 28 days. The test sample was a cuboid with dimensions of 40 × 40 × 160 mm³. Three samples were tested for each mixing ratio, and the results were averaged.

The resistivity test was performed using a portable nondestructive resistivity tester (Proceq, Switzerland). According to the AASHTO T 358 standard [31], resistivity experiments were conducted on cylinders with dimensions of Φ100 × 200 mm at curing ages of 3, 7, and 28 days. Each sample was tested thrice, and the results were averaged.

2.3.4 Microscopic characterization

Test samples for thermogravimetric analysis (TGA), XRD, and FTIR were dehydrated by solvent exchange [32]. Manual grinding with a small amount of isopropyl alcohol was performed in an agate mortar to prevent carbonation during the grinding. After grinding, the mixture was poured into a beaker, and isopropanol that is approximately four times the mass of the mixture was added; the mixture was allowed to stand for 10 min. The suspension was then filtered and washed four times alternately with isopropanol and diethyl ether. Finally, the filtered powder was dried in a vacuum drying oven. The tests were performed the following day.

TGA was performed using an SDT Q600 TA Instruments instrument with a ramp rate of 10 °C/min to measure mass loss in the range 20–1000 °C. Anitrogen purge at a gas flow rate of 100 mL/min was used during the test. XRD was performed using an X'Pert-pro MPD diffractometer from 5 to 70° (2 θ) in steps of 0.013° . ATR-FTIR experiments were performed using a Frontier spectrometer (PerkinElmer) in the scan range 500–4000 cm⁻¹, scanning each sample 16 times.

3. Results and discussion

3.1 Heat of hydration

Figures 3a and 3b show the 7-day heats of hydration and cumulative hydration, respectively. The start time of the acceleration period occurred earlier in the pastes with CC addition than in the control group (CC0), as seen in the enlarged view in Figure 3a. The time to peak of heat flow gradually moved forward with an increased CC addition. As also seen in the enlarged view in Figure 3b, the cumulative heat release of the mixed paste with added CC was higher than that of the control group (CC0) in the early stage of hydration (before 40 h). CC accelerated the hydration rate of the paste, which was attributed to the dilution and nucleation effects of CC [33].

Because the cement content in CC4 and CC6 pastes was lower than that in CC0, the cumulative heat release of CC0 gradually exceeded that of CC2, CC4, and CC6 at approximately 36 h. This heat release difference suggested that the physical action (filling effect) produced by CC had a significant impact only in the early stages of hydration. Figure 4 shows the normalized heat of hydration and the cumulative heat based on the cement. The heat of hydration of the mixed paste with added CC was higher than that of the control group because the filling effect (dilution effect nucleation effect) produced by CC enhanced the hydration reaction of the cement [34].

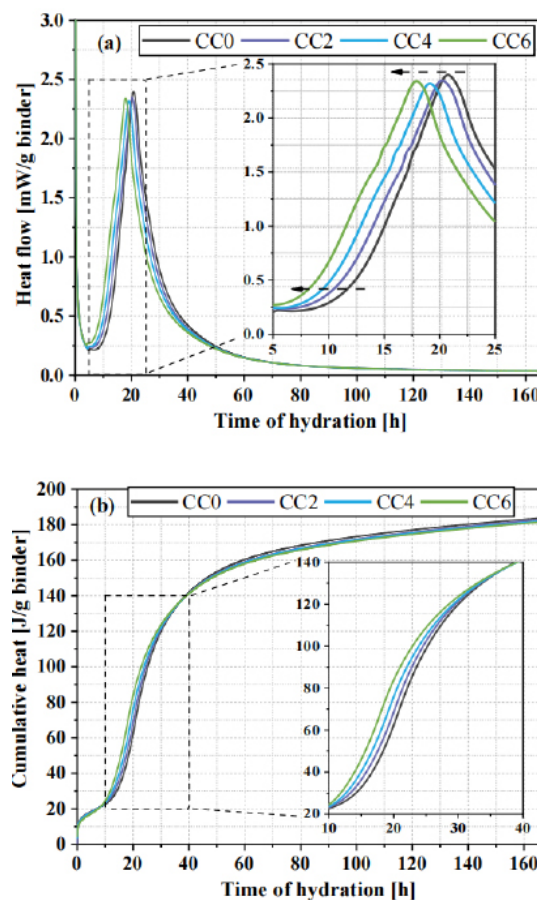


Figure 3. (a) Heat of hydration and (b) cumulative heat of pastes based on the binder.

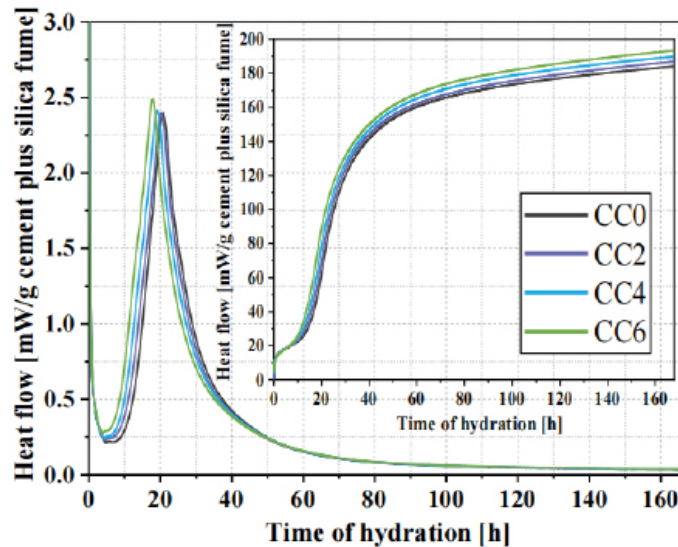


Figure 4. Normalized heat of hydration and cumulative heat based on the cement plus silica fume.

3.2 Mechanical properties

The compressive (3, 7, and 28 days) and flexural strength (28 days) test results of the mortars are shown in Figure 5a. Figure 5b shows the normalized compressive strength of the mortars with CC0 as the benchmark. From Figure 5a, the compressive strength of the mortars added with CC was higher than that of the control group CC0 when the curing age was 3 d. Adding 2 and 4% CC significantly improved the 3-day compressive strength of the mortar. The compressive strengths of CC2 and CC4 reached 71.91 and 72.71 MPa, respectively. The 3-day compressive strength of the mortars increased because of the filler and nucleation effects caused by the addition of CC [29]. The presence of CC improved particle packing and refined the internal pores of the mortar. CC provided nucleation sites for hydration products, accelerating the mortar hydration rate [35] [36]. The heat of hydration results also showed that the presence of CC accelerated the paste hydration rate. Notably, the 3-day compressive strength values of CC6 were very close to those of the control group. The physical effect produced by adding CC contributed to the development of the early compressive strength of the mortar. However, the reduction in hydration products due to the decreased cement and SF content also significantly affected the development of the compressive strength in the middle and late periods (7 days and 28 days). When the curing age reached 28 days, the compressive strength of CC2 was slightly higher than that of the control group (112.94 MPa). The compressive strengths of both CC4 and CC6 were lower than that of CC0. Similar findings have been reported previously [37] [38]. Kang et al. [39] found that the presence of LP in the paste led to capillary pores of approximately 10 nm, leading to a decreased UHPC compressive strength in the middle and late stages (28 days). With an increased curing age, the gradual weakening of the physical effect of CC may have been one of the reasons.

In addition to physical impacts, CC has chemical effects and a coupling effect with aluminum-rich SCMs [40]. However, aluminum-rich SCMs were not added in this study; thus, CC did not significantly contribute to developing the compressive strength in the middle and late stages of the mortar. Figure 5b further shows that when compared to the control group CC0, the normalized compressive strength percentage of the mortar supplemented with CC steadily declined with increasing curing age. With an increased CC addition, the normalized compressive strength percentage of the mortar decreased significantly.

The results for the 28-day flexural strength test of the mortar are shown in Figure 5a. The flexural strength of CC0 in the control group was the lowest at 10.12 MPa; the flexural strength of CC2 was the highest at 11.74 MPa. A correlation analysis was performed on the cumulative heat release and compressive strength for 3 and 7 days, as shown in Figure 6. An excellent linear relationship between them ($R^2 = 0.932$) was observed.

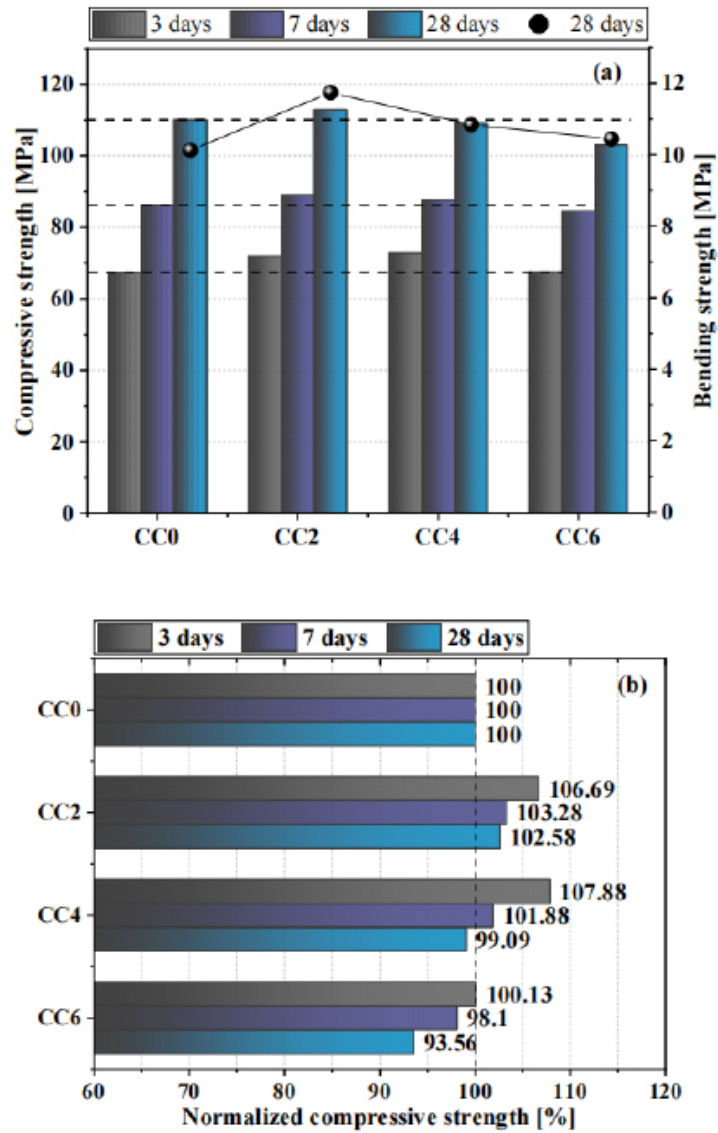


Figure 5. (a) Compressive and flexural strength; (b) normalized compressive strength of the samples.

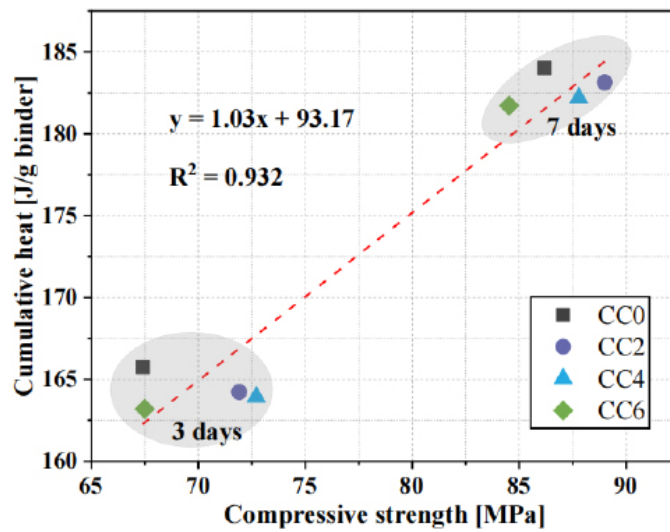


Figure 6. Compressive strength and cumulative heat relationship.

3.3 Ultrasonic pulse velocity

Figure 7 shows the ultrasonic pulse velocity (UPV) results after 3, 7, and 28 days. When the curing age was 3 days, the UPV of CC0 was 4.348 km/s, and the UPV of the mortars with added CC was higher than that of CC0. CC4 had the highest UPV (4.469 km/s). The addition of CC produced filler and dilution effects. The presence of CC improved particle packing, refined the internal pores of the mortar, and accelerated the mortar hydration rate. The resulting hydration products made the microstructure of the mortar denser [39] [41]. With an increased curing time, the UPV of the mortar also gradually increased. At 7 days, the UPV of the mortar with added CC was still higher than that of the control CC0. However, compared with the control group, the UPV of the mortars with added CC was only approximately 0.84–1.31% higher than that of CC0. When the curing age reached 28 days, the UPV of CC6 was lower than that of CC0.

The UPV growth rate was calculated using the following formula (1):

$$\text{Growth rate of UPV (\%)} = \frac{U_T - U_{3d}}{U_{3d}} \times 100 \quad (1)$$

where U_T and U_{3d} are the UPV values when the curing age is 7 or 28 days and 3 days, respectively. The results are shown in Figure 8a. With an increased CC substitution, the growth rate of UPV gradually decreased. Adding CC had a significant effect on the mortars in the early stage, accelerating the hydration rate and making the interior of the mortar dense through the hydration products produced [35]. With an increased curing time, the physical effect of CC in the early stage gradually decreased. On the contrary, the effect of decreased cement and SF content gradually became significant. In addition, a quantitative correlation analysis was performed between the growth rate of UPV and CC content, as shown in Figure 8b. An excellent linear relationship between the growth rate of UPV and CC content was observed, and the growth rate of UPV decreased with increased CC content. In addition, the coefficient of determination (0.958) between the growth rate and CC content of UPV from 3 to 28 days was higher than the coefficient of determination (0.845) between the growth rate and CC content of UPV from 3 to 7 days. The differences proved that CC had an effect on the UPV development of mortar in the early stage, with the effect gradually decreasing with increasing curing time.

Solid hydration products have a significant effect on the development of mortar UPV; the development of compressive strength is also affected by the content of the solid hydration products. Figure 9 shows the quantitative correlation analysis between the compressive strength and UPV. There was an excellent exponential relationship between compressive strength and UPV in this study ($R^2 = 0.897$).

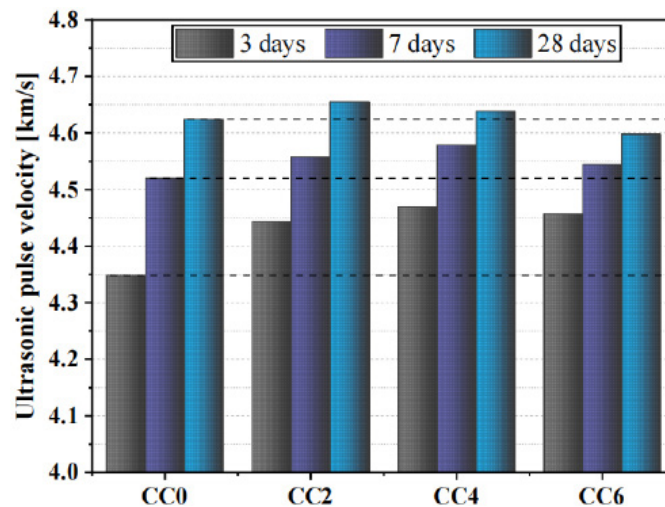


Figure 7. Ultrasonic pulse velocity results.

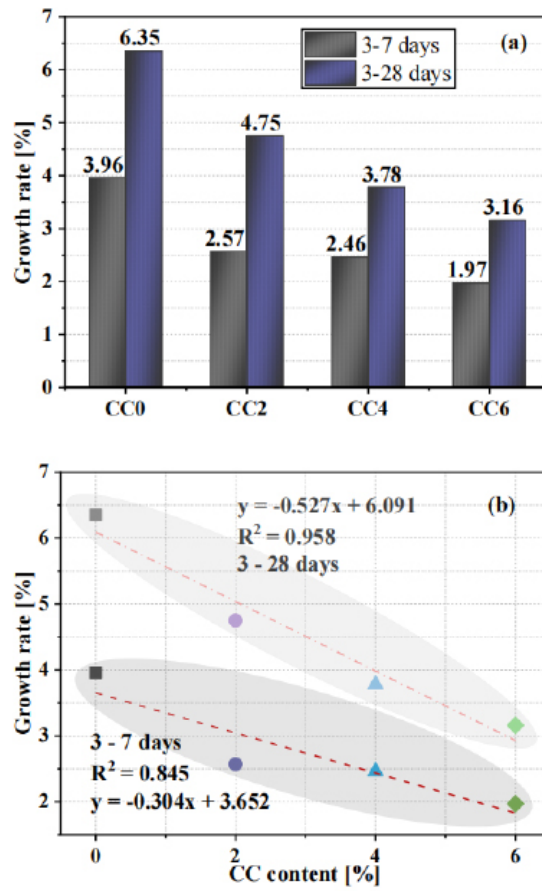


Figure 8. (a) Ultrasonic pulse velocity growth rate at 3-7 and 3-28 days; (b) the relationship between UPV growth rate and CC content.

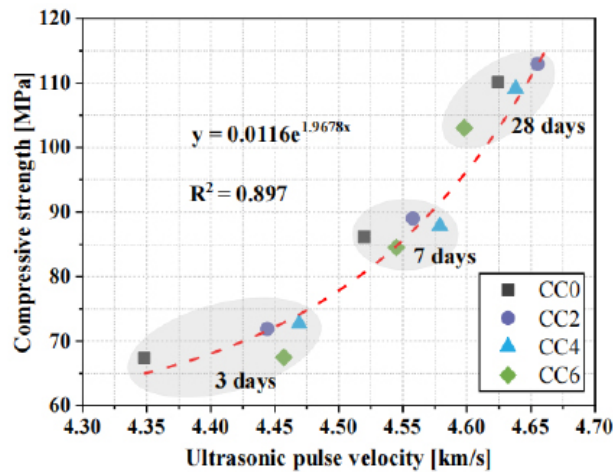


Figure 9. Relationship between ultrasonic pulse velocity and compressive strength.

3.4 Electrical resistivity

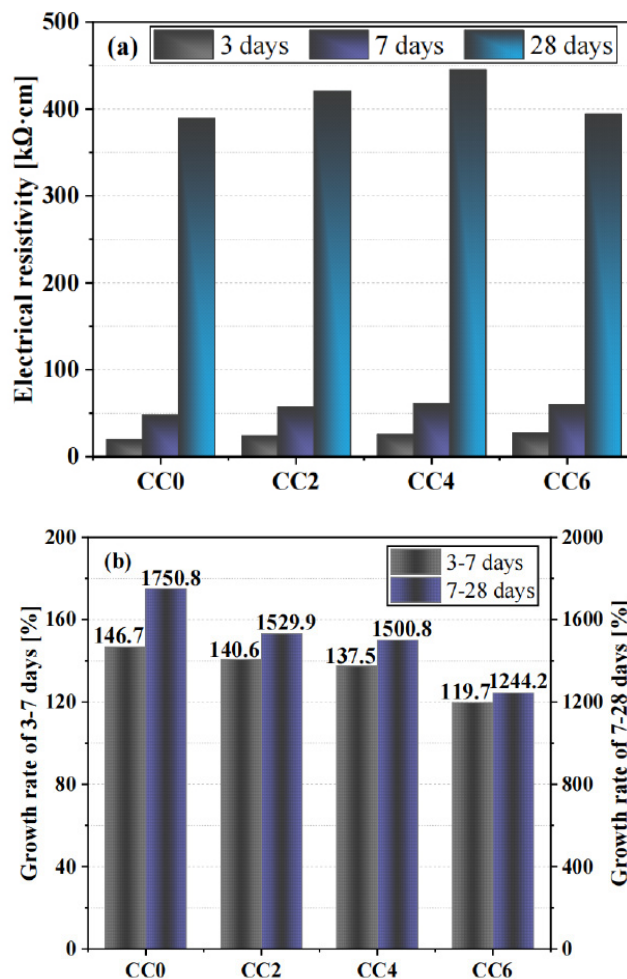
The resistivity test results at 3, 7, and 28 days in this study are shown in Figure 10a. When the curing age was 3 days, the resistivity of the mortar was between 19.5 and 26.95 kΩ·cm; the resistivity of CC0 was the smallest (19.5 kΩ·cm), and the resistivity of CC6, the most CC content, was the largest (26.95 kΩ·cm). With increased curing age, the resistivity of mortar at 28 days ranged from 389.5 to 445 kΩ·cm. Notably, the resistivity increase of all mortar samples was slight from 3 to 7 days. A significant increase in resistivity from that

of 7 days curing was observed when the curing time reached 28 days. The growth rate of the resistivity was calculated using the following formula (2):

$$\text{Growth rate of ER (\%)} = \frac{R_T - R_t}{R_t} \times 100 \tag{2}$$

where R_T is the resistivity when the curing is 7 or 28 days, and R_t is the resistivity when the curing is 3 or 7 days. The results are shown in Figure 10b. The resistivity growth rate in the middle and late periods (7–28 days) was much higher than that in the early and middle periods (3–7 days) because the pozzolanic reaction of SF produced more CSH in the middle and late stages, making the internal microstructure of the mortar denser [42]. In addition, as shown in Figure 10b, with increased CC content, both the 3–7 and 7–28 days resistivity growth rates of the mortar gradually decreased. The trend may be due to the reduced cement and SF content.

The resistivity of the CC-added mortar was normalized to that of the control group (CC0), as shown in Figure 10c. As the curing time increased, the resistivity difference between the mortars became less significant. After 3 days, the resistivity of the mortars with added CC was higher than that of CC0. The resistivity of the mortars also gradually increased with increasing CC content. The resistivity of the mortars with added CC was 21.8–38.21% higher than the control group, which was attributed to the physical action of CC (filler and dilution actions) [43]. With an increased curing time, the effect of the physical action of CC on the resistivity of the mortars gradually decreased. At 7 days, the resistivity of the mortars with added CC was 18.82–26.4% higher than that of the control CC0. When the curing age reached 28 days, the resistivity of the mortars with added CC was only 1.28–14.25% higher than that of CC0.



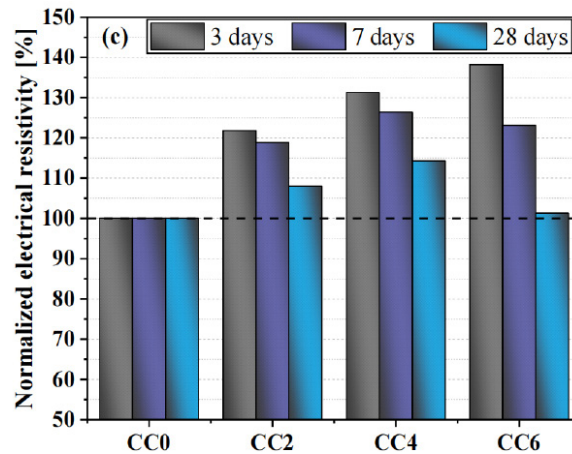
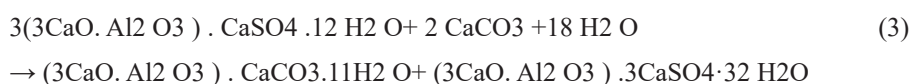


Figure 10. (a) Electrical resistivity test results; (b) electrical resistivity growth rate at 3–7 and 7–28 days; (c) electrical resistivity normalized to the resistivity of CC0.

3.5 XRD

Figures 11a and 11b show the XRD patterns measured at 3 and 28-day curing, respectively. The CH diffraction peak of the paste increased gradually with an increased amount of CC, consistent with the results of the heat of hydration experiment, in which CC accelerated the hydration rate of the paste. With an increased CC addition, the diffraction peaks of CC also increased. In addition, because the Korean cement used in this study contained 2–3% CaCO₃ [44], the diffraction peaks of CC was also observed in the XRD pattern of CC0. With an increased curing time, the crystalline phase in the paste changed significantly.

Compared to the XRD pattern of the paste after 3 days, the diffraction peaks ($2\theta = 9.1$ and 15.9°) of ettringite in the paste increased significantly after 28 days. The diffraction peaks of hemicarboaluminate (Hc) and monocarboaluminate (Mc) are shown in Figure 11b. According to a previous study [45], CC was beneficial for the production of carboaluminate and ettringite, as shown in reaction (3).



Comparing Figures 11a and 11b, the intensity of the diffraction peaks caused by the C3S and C2S in the pastes decreased as the curing time increased. Compared with the XRD pattern of the paste after 3 days, the diffraction peaks of CH ($2\theta = 17$ and 34°)

at 28 days were significantly reduced. The reduction may be due to some CH being consumed by the pozzolanic reaction in SF in the middle and late stages.

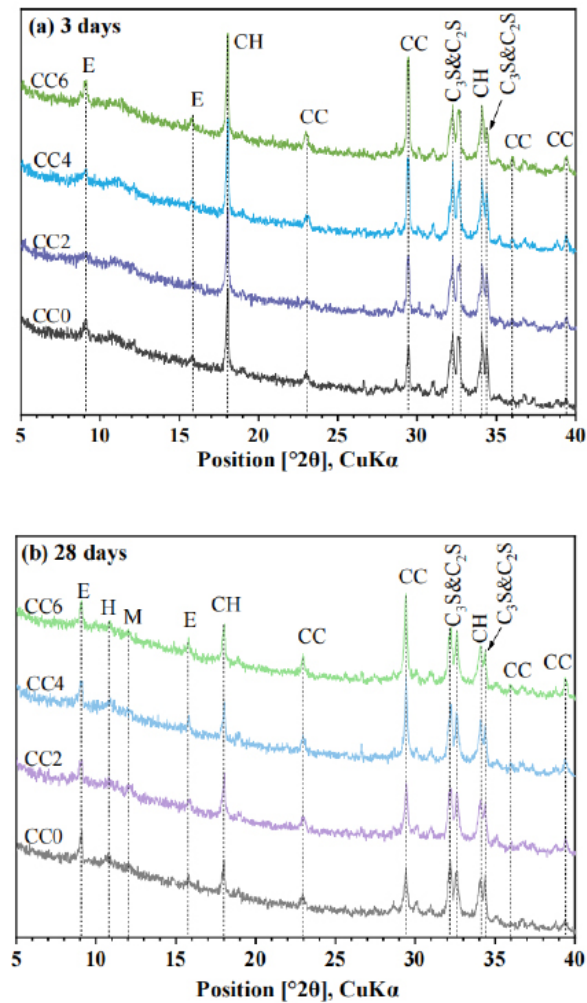


Figure 11. XRD patterns of the pastes at (a) 3 days and (b) 28 days. E = Ettringite; H = Hemicarboaluminate; M = Monocarboaluminate; CH = calcium hydroxide; CC = Calcium carbonate.

3.6 ATR-FTIR

Figures 12a and 12b show the ATR-FTIR spectra of the pastes after 3 and 28 days of curing, respectively. The absorption peak caused by the OH⁻ (ν) stretching vibration in CH appeared at 3641 cm⁻¹ [46] [47]. The CH- absorption peak at 28 days for the paste in Figure 12b was very small compared to that in Figure 12a, consistent with the XRD results because of the pozzolanic reaction in the SF in the middle and late stages.

The broad peak at 1451 cm⁻¹ was caused by the asymmetric stretching vibration of CO₃²⁻ (ν₃) in CaCO₃ [48]. In addition, the absorption peaks at 877 and 715 cm⁻¹ were caused by the out-of-plane bending vibrations of CO₃²⁻ (ν₂ and ν₄) and CaCO₃, respectively [46] [47]. The absorption peak caused by CO₃²⁻ increased with increased CC content in the paste. In addition, the absorption peaks caused by CO₃²⁻ decreased with an increased curing age because part of the CC and aluminate generated Hc and Mc, which was also observed in the XRD patterns. The absorption peak at 1116 cm⁻¹ was caused by SO₄²⁻ (ν₃) stretching vibration [48] [49]. As shown in Figure 12a, the absorption peak of the CC-added paste was significantly larger than that of CC0. In addition, compared with that at 3 days, the SO₄²⁻ absorption peak of the paste at 28 days decreased significantly with an increased curing time. The absorption peak caused by the SiO₄²⁻ (ν₃) asymmetric stretching vibration of CSH appeared at 952 cm⁻¹ [46]. From Figure 12a, the absorption peak of the paste containing CC was significantly larger than that of CC0 because the

physical action early produced by the CC accelerated the hydration rate of the paste. In addition, comparing Figures 12a and 12b, it can be observed that the absorption peak at 952 cm^{-1} increased as the curing time increased.

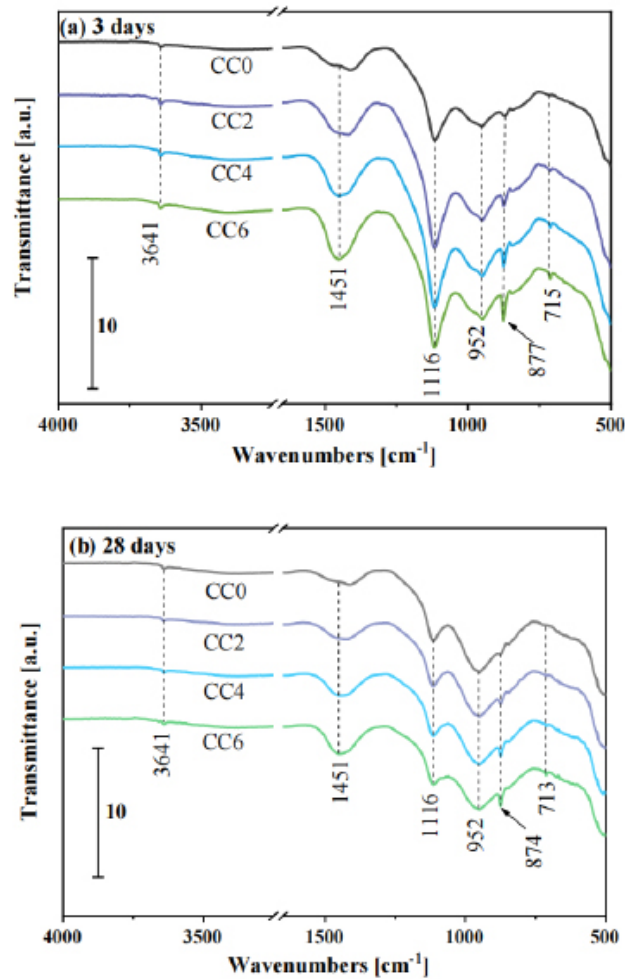


Figure 12. ATR-FTIR spectra of the pastes at (a) 3 and (b) 28 days.

3.7 TGA

Figures 13a and 13b show the results of the TG analysis of the pastes at 3 and 28 days. Three stages of weight loss was observed: (1) hydration product (calcium silicate hydrate, AFt, and AFm) decomposition (100–200 °C)[50], (2) calcium hydroxide decomposition (400–500 °C) [50], and (3) CaCO_3 decomposition (600–750 °C)[32]. During the first weight-loss stage, the hydration products formed in the paste containing CC were higher than those of the control group CC0, and the peak weight loss increased with increased CC addition, as seen in Figure 13a. In addition, in the second stage, it was found that the CH content in the paste with added CC was also higher than that of CC0, confirming that the CC had a physical effect in the early stages, which accelerated the hydration rate of the paste. When the curing time reached 28 days, the decomposition peak of the hydration products increased significantly during the first stage of weight loss. With an increased curing time, the continuous hydration of cement generated more hydration products. In addition, the pozzolanic reaction of SF consumed CH, generating a large amount of calcium silicate hydrate. In Figure 13b, the CH decomposition peak at approximately 450 °C was significantly lower than that at 3 days. In addition, the decomposition peak of the CCO paste at about 120 °C exceeded that of the paste containing CC. This was due to the reduced cement content in the CC-containing pastes. The presence of CC can accelerate the hydration rate of the paste in the early stage; however, because of the extremely low reactivity of CC, a large number of hydration products cannot be generated in the middle

and later stages of hydration.

The chemically bound water content was calculated according to the method described by De Weerd [51], as shown in Equation (4):

$$W_b = \frac{W_{40} - W_{550}}{W_{550}} \times 100\% \tag{4}$$

The results are shown in Table 3. At 3 days, the chemically bound water content in the paste increased with the CC content. Initially, CC accelerated the hydration rate of the paste; thus, the hydration products also increased. At day 28, the chemically bound water of CC0 increased significantly compared to that at day 3. With an increased curing time, the cement continued to undergo a hydration reaction, and SF also experienced a pozzolanic reaction; thus, the hydration products increased significantly. In the middle and late stages, the physical effect of the CC gradually decreased, and the influence of decreased cement content in the paste gradually increased. A quantitative correlation analysis between compressive strength and chemically bound water (Wb) was also performed, as shown in Figure 14. An excellent linear relationship was observed between them ($R_2 = 0.933$).

Table 3. Chemically bound water content in the pastes (%).

Curing time	CC0	CC2	CC4	CC6
3 days	11.84	12.26	12.29	12.82
28 days	15.85	16.08	14.81	14.50

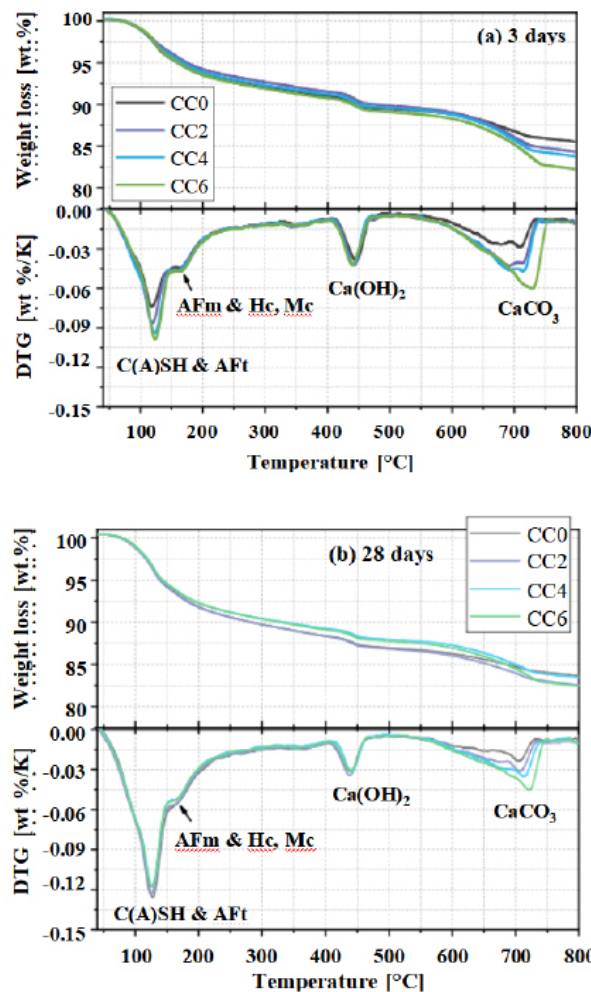


Figure 13. TGA and DTG curves for the pastes at (a) 3 and (b) 28 days.

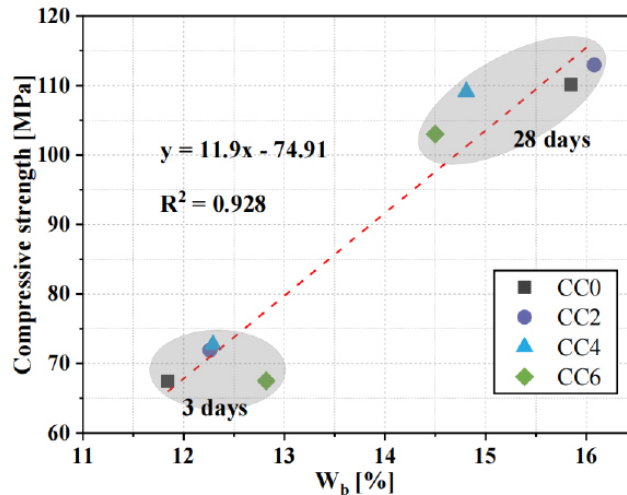


Figure 14. Relationship between Wb and compressive strength.

3.8 Sustainability

The CO₂ emission for the production of calcium carbonate is determined as follows. The CO₂ emission per kilogram of CH is 0.528 kgCO₂/kg [52]. When CH was used to prepare CC in this study, the chemical reaction formula (5) was as follows:



One kilogram of CC consumes 0.74 kg CH and 0.44 kg CO₂; thus, the CO₂ emission factor of CC is 0.74 × 0.528 = 0.39072 kg·CO₂/kg.

CO₂ emissions are currently a topic of concern, and the addition of SF and CC in concrete has a positive effect in reducing CO₂ emissions. Therefore, the CO₂ emission reduction capacity of UHPC was calculated. The CO₂ emissions per cubic meter of concrete were calculated according to the method described by Zhang et al. [53], as shown in formulas (6) and (7):

$$\sum_{i=1}^n \frac{M_i}{\rho_i} = 1 \tag{6}$$

$$\text{CO}_{2/m^3} = \sum_{i=1}^n (M_i \times \text{CO}_{2(i)}) \tag{7}$$

where ρ_i represents the specific gravity of the raw materials; M_i is the mass of raw materials (kg/m³), as shown in Table 4; CO_{2/m³} represents the CO₂ emissions per cubic concrete; CO_{2(i)} represents the CO₂ emissions per kilogram of raw material, as shown in Table 5.

Table 4. The mass of the different components and CO₂ emissions of mortars.

NO.	Mass of raw materials (kg/m ³)						CO ₂ emissions (kg·CO ₂ /m ³)
	OPC	SF	CC	Water	SP	Sand	
CC0	910.57	160.69	0.00	214.25	21.43	1071.26	790.90
CC2	891.67	157.35	21.41	214.09	21.41	1070.44	773.49
CC4	872.80	154.02	42.78	213.92	21.39	1069.61	756.10
CC6	853.96	150.70	64.13	213.76	21.38	1068.79	738.74



Table 5. CO₂ emission factors for raw materials[54] [55].

	OPC	SF	CC	SP	Water	Sand
CO ₂ emission factor (kg. CO ₂ /kg)	0.863	0.014	-0.04928	0.0016	0.000196	0.0026

The calculation results of CO_{2/m³} are shown in Table 4. The CO₂ emissions decreased with the addition of CC. This is predictable because the substitution of CC reduces the use of other raw materials, and the CO₂ emissions per unit of CC are negative.

The CO₂ emissions of the mortars were compared with the compressive strength and resistivity (durability performance) at 28 days to better understand the long-term performance of the concrete. The CO₂ emissions per unit compressive strength and resistivity were computed using Equations (7) and (8), respectively.

$$CO_{2-c} = \frac{CO_{2/m^3}}{F_{c-28}} \tag{7}$$

$$CO_{2-e} = \frac{CO_{2/m^3}}{F_{e-28}} \tag{8}$$

The calculation results of CO_{2-c} (CO₂ emission per unit compressive strength, kg·CO₂/MPa) and CO_{2-e} (CO₂ emission per unit resistivity, kg·CO₂/kΩ·cm) are shown in Figure 15. The CO_{2-c} and the CO_{2-e} of the mortar with CC were both smaller than those of CC0. The CO_{2-c} of CC2 was the smallest at 6.85 kg·CO₂/MPa. Because the addition of CC diminished the later compressive strength of the mortar, the CO_{2-c} of CC4 was equivalent to that of CC0. Compared to the control group, the CO_{2-e} of the mortar supplemented with the different CC additions reduced by 9.36, 16.26, and 7.88%, respectively. CC4 exhibited the lowest value at only 1.70 kg·CO₂/kΩ·cm.

Based on the results, the addition of CC to the mixture had dilution and nucleation effects, accelerating the hydration reaction rate and contributing to the early compressive strength development. However, with an increased curing time, the physical effect of CC gradually decreased. Simultaneously, the effect of reducing the cement and silica fume content gradually increased (decreased hydration products).

The decrease in hydration products decreased the compressive strength and resistivity of the mixtures with high CC content when the curing age reached the middle and late stages. However, adding CC reduced the CO₂ emissions of the mixture, and a high amount of CC affected the later development of the compressive strength and resistivity of the mixture. Therefore, when the compressive strength and resistivity were considered simultaneously, adding CC within 4% was the most cost-effective. It can also ensure that the mechanical properties and durability of the mixture are maintained while minimizing CO₂ emissions.

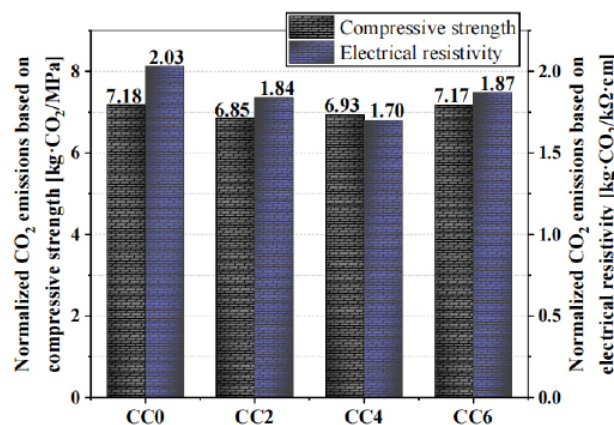


Figure 15. CO₂ emissions per unit of electrical resistivity and compressive strength.



4. Conclusion

This study investigated the addition of CO₂ to UHPC using an indirect addition method. Gaseous CO₂ was first converted into solid CaCO₃ and then added to the UHPC. The performance and sustainability of UHPC were investigated experimentally. The mortars were tested for their compressive strength, flexural strength, ultrasonic strength, and resistivity. The heat of hydration and microstructures of the pastes were also characterized. The following conclusions were drawn from the test results.

(1) The hydration heat and strength test results showed that adding CO₂ converted into a solid (calcium carbonate) accelerated the early hydration rate of UHPC, contributing to improved early compressive strength. After normalizing the compressive strength based on the control group, it was found that the percentage of compressive strength of the UHPC sequestered with CO₂ gradually decreased with increased curing age.

(2) UPV experiments showed that the physical effect of adding CO₂ (CC) converted into a solid gradually decreased during the early stage. With an increased curing time, the UPV growth rate decreased with an increased CC content. Moreover, an excellent exponential relationship between UPV and compressive strength ($R^2 = 0.897$) was observed.

(3) The surface resistivity tests showed that the resistivity growth rate (1244.2–1750.8%) of UHPC in the middle and late stages (from 7 to 28 days) was much higher than that in the early and middle stages (from 3 to 7 days) (119.7–146.7%); however, the resistivity difference between the mortars became less significant as the curing time increased. Adding CC converted into a solid-state significantly affected the early resistivity. However, in the middle and late stages, cement hydration and the pozzolanic reaction of SF had a more significant impact on the resistivity of the mortar.

(4) The XRD and FTIR test results showed that the pozzolanic reaction of SF had a gradually significant effect on the paste in the middle and late stages. In addition, at 28 days, the presence of Hc and Mc was observed in the XRD pattern owing to the chemical reaction of CC with the aluminum phase in the cement.

(5) The results of the TGA experiments showed that the decomposition peak of CSH increased with an increased CC content at 3 days. This indicated that CC accelerated the hydration rate of the paste. In addition, an excellent linear relationship between chemically bound water and compressive strength ($R^2 = 0.933$) was observed.

(6) Compared with the control group, the CO₂ emissions per unit compressive strength and per unit resistivity of the mortar added with CC decreased to varying degrees, suggesting indirect capture and storage of CO₂ in UHPC was feasible. In addition, when the compressive strength and resistivity were considered simultaneously, the addition of CC within 4% was the most cost-effective. The mechanical properties and durability of the mixture were maintained while minimizing the CO₂ emissions.

Acknowledgement

This study was supported by the National Research Foundation of Korea (grant number NRF-2020R1A2C4002093).

Author contributions

Yi-Han: Conceptualization, Methodology, Investigation, Data curation, Writing - review & editing.

Run-Sheng Lin: Investigation, Writing - review & editing.

Xiao-Yong Wang: Conceptualization, Supervision, Validation, Resources, Project administration, Funding acquisition, Writing - review & editing.

Conflict of interest

The authors state no conflict of interest.

References

- He Z H, Shen M L, Shi J Y, Yalcinkaya C, Du S G, Yuan Q. Recycling coral waste into eco-friendly UHPC: Mechanical strength, microstructure, and environmental benefits. *Sci Total Environ.* 2022; 836: 155424. doi: 10.1016/j.scitotenv.2022.155424.
- Huang H, Gao X, Khayat K H. Contribution of fiber orientation to enhancing dynamic properties of UHPC under impact loading. *Cement and Concrete Composites.* 2021; 121: 104108. doi: 10.1016/j.cemconcomp.2021.104108.
- Ren M, Wen X, Gao X, Liu Y. Thermal and mechanical properties of ultra-high performance concrete incorporated with microencapsulated phase change material. *Construction and Building Materials.* 2021; 273: 121714. doi: 10.1016/j.conbuildmat.2020.121714.
- Mo Z, Gao X, Su A. Mechanical performances and microstructures of metakaolin contained UHPC matrix under steam curing conditions. *Construction and Building Materials.* 2021; 268: 121112. doi: 10.1016/j.conbuildmat.2020.121112.
- Harrison E, Berenjian A, Seifan M. Recycling of waste glass as aggregate in cement-based materials. *Environmental Science and Ecotechnology.* 2020; 4: doi: 10.1016/j.ese.2020.100064.
- Bajaber M A, Hakeem I Y. UHPC evolution, development, and utilization in construction: a review. *Journal of Materials Research and Technology.* 2021; 10: 1058-1074. doi: 10.1016/j.jmrt.2020.12.051.
- Zhang G Y, Ahn Y H, Lin R S, Wang X Y. Effect of Waste Ceramic Powder on Properties of Alkali-Activated Blast Furnace Slag Paste and Mortar. *Polymers (Basel).* 2021; 13: 13162817. doi: 10.3390/polym13162817.
- Isaia G C, GASTALDI A L G, Moraes R J C, composites c. Physical and pozzolanic action of mineral additions on the mechanical strength of high-performance concrete. 2003; 25: 69-76.
- Ghafari E, Ghahari S A, Costa H, Júlio E, Portugal A, Durães L. Effect of supplementary cementitious materials on autogenous shrinkage of ultra-high performance concrete. *Construction and Building Materials.* 2016; 127: 43- 48. doi: 10.1016/j.conbuildmat.2016.09.123.
- Liu Z, Meng W. Fundamental understanding of carbonation curing and durability of carbonation-cured cement-based composites: A review. *Journal of CO2 Utilization.* 2021; 44: 101428. doi: 10.1016/j.jcou.2020.101428.
- Liu B, Qin J, Shi J, Jiang J, Wu X, He Z. New perspectives on utilization of CO2 sequestration technologies in cement-based materials. *Construction and Building Materials.* 2021; 272: 121660. doi: 10.1016/j.conbuildmat.2020.121660.
- He J, Li Z, Zhang X, Wang H, Dong W, Du E, et al. Towards carbon neutrality: A study on China's long-term low-carbon transition pathways and strategies. *Environmental Science and Ecotechnology.* 2022; 9: 100134. doi: 10.1016/j.ese.2021.100134.
- Duan L, Hu W, Deng D, Fang W, Xiong M, Lu P, et al. Impacts of reducing air pollutants and CO2 emissions in urban road transport through 2035 in Chongqing, China. *Environmental Science and Ecotechnology.* 2021; 8: 100125. doi: 10.1016/j.ese.2021.100125.
- Tian S, Wang S, Bai X, Luo G, Li Q, Yang Y, et al. Global patterns and changes of carbon emissions from land use during 1992–2015. *Environmental Science and Ecotechnology.* 2021; 7: 100108. doi: 10.1016/j.ese.2021.100108.
- Di Maria A, Snellings R, Alaerts L, Quaghebeur M, Van Acker K. Environmental assessment of CO2 mineralisation for sustainable construction materials. *International Journal of Greenhouse Gas Control.* 2020; 93: 102882. doi: 10.1016/j.ijggc.2019.102882.

- Hepburn C, Adlen E, Beddington J, Carter E A, Fuss S, Mac Dowell N, et al. The technological and economic prospects for CO₂ utilization and removal. *Nature*. 2019; 575: 87-97. doi: 10.1038/s41586-019-1681-6.
- Norhasyima R S, Mahlia T M I. Advances in CO₂ utilization technology: A patent landscape review. *Journal of CO₂ Utilization*. 2018; 26: 323-335. doi: 10.1016/j.jcou.2018.05.022.
- Raza A, Gholami R, Rezaee R, Rasouli V, Rabiei M. Significant aspects of carbon capture and storage – A review. *Petroleum*. 2019; 5: 335-340. doi: 10.1016/j.petlm.2018.12.007.
- Lee H-S, Lim S-M, Wang X-Y. Optimal Mixture Design of Low-CO₂ High- Volume Slag Concrete Considering Climate Change and CO₂ Uptake. *International Journal of Concrete Structures and Materials*. 2019; 13. doi: 10.1186/s40069-019-0359-7.
- Rostami V, Shao Y, Boyd A J J J o m i C E. Carbonation curing versus steam curing for precast concrete production. 2012; 24: 1221-1229.
- Ashraf W. Carbonation of cement-based materials: Challenges and opportunities. *Construction and Building Materials*. 2016; 120: 558-570. doi: 10.1016/j.conbuildmat.2016.05.080.
- Chen T, Gao X. Effect of carbonation curing regime on strength and microstructure of Portland cement paste. *Journal of CO₂ Utilization*. 2019; 34: 74-86. doi: 10.1016/j.jcou.2019.05.034.
- Qian X, Wang J, Fang Y, Wang L. Carbon dioxide as an admixture for better performance of OPC-based concrete. *Journal of CO₂ Utilization*. 2018; 25: 31-38. doi: 10.1016/j.jcou.2018.03.007.
- Saillio M, Baroghel-Bouny V, Pradelle S, Bertin M, Vincent J, d'Espinose de Lacaillerie J-B. Effect of supplementary cementitious materials on carbonation of cement pastes. *Cement and Concrete Research*. 2021; 142: 106358. doi: 10.1016/j.cemconres.2021.106358.
- Justnes H, Skocek J, Østnor T A, Engelsen C J, Skjølvold O. Microstructural changes of hydrated cement blended with fly ash upon carbonation. *Cement and Concrete Research*. 2020; 137: 106192. doi: 10.1016/j.cemconres.2020.106192.
- Qin L, Gao X, Li Q. Upcycling carbon dioxide to improve mechanical strength of Portland cement. *Journal of Cleaner Production*. 2018; 196: 726-738. doi: 10.1016/j.jclepro.2018.06.120.
- Han Y, Lin R, Wang X-Y. Performance of sustainable concrete made from waste oyster shell powder and blast furnace slag. *Journal of Building Engineering*. 2022; 47: 103918. doi: 10.1016/j.jobe.2021.103918.
- ASTM C349, Standard Test Method for Compressive Strength of Hydraulic- Cement Mortars (Using Portions of Prisms Broken in Flexure), ASTM International, West Conshohocken, PA, 2018.
- ASTM C78, Standard test method for flexural strength of concrete (using simple beam with third-point loading), ASTM International, West Conshohocken, PA, 2018.
- ASTM C597-16, Standard Test Method for Pulse Velocity through Concrete, ASTM International, West Conshohocken, PA, 2016.
- AASHTO T 358, Standard Method of Test for Surface Resistivity Indication of Concrete's Ability to Resist Chloride Ion Penetration, American Association of State Highway and Transportation Officials, Washington, DC, 2015.
- Lin R-S, Han Y, Wang X-Y. Macro-meso-micro experimental studies of calcined clay limestone cement (LC3) paste subjected to elevated temperature. *Cement and Concrete Composites*. 2021; 116: 103871. doi: 10.1016/j.cemconcomp.2020.103871.
- Han Y, Lin R, Wang X-Y. Performance and sustainability of quaternary composite paste comprising limestone, calcined Hwangtoh clay, and granulated blast furnace slag. *Journal of Building Engineering*. 2021; 43: 102655. doi: 10.1016/j.jobe.2021.102655.
- Berodier E, Scrivener K J J o t A C S. Understanding the Filler Effect on the Nucleation and Growth of C^sCH. 2014; 97: 3764-3773.
- Lothenbach B, Le Saout G, Gallucci E, Scrivener K. Influence of limestone on the hydration of Portland

- cements. *Cement and Concrete Research*. 2008; 38: 848-860. doi: 10.1016/j.cemconres.2008.01.002.
- Ge Z, Tawfek A M, Zhang H, Yang Y, Yuan H, Sun R, et al. Influence of an extrusion approach on the fiber orientation and mechanical properties of engineering cementitious composite. *Construction and Building Materials*. 2021; 306: 124876. doi: 10.1016/j.conbuildmat.2021.124876.
- Bonavetti V, Donza H, Menendez G, Cabrera O, Irassar E J C, Research C. Limestone filler cement in low w/c concrete: A rational use of energy. 2003;33: 865-871.
- Vuk T, Tinta V, Gabrovšek R, Kaučič V J C, Research c. The effects of limestone addition, clinker type and fineness on properties of Portland cement. 2001; 31: 135-139.
- Kang S-H, Jeong Y, Tan K H, Moon J. The use of limestone to replace physical filler of quartz powder in UHPFRC. *Cement and Concrete Composites*. 2018;94: 238-247. doi: 10.1016/j.cemconcomp.2018.09.013.
- Dhandapani Y, Santhanam M, Kaladharan G, Ramanathan S. Towards ternary binders involving limestone additions — A review. *Cement and Concrete Research*. 2021; 143: 106396. doi: 10.1016/j.cemconres.2021.106396.
- Zhang H, Xu Y, Gan Y, Chang Z, Schlangen E, Šavija B. Combined experimental and numerical study of uniaxial compression failure of hardened cement paste at micrometre length scale. *Cement and Concrete Research*. 2019; 126: 105925. doi: 10.1016/j.cemconres.2019.105925.
- Ghoddousi P, Adelzade Saadabadi L. Study on hydration products by electrical resistivity for self-compacting concrete with silica fume and metakaolin. *Construction and Building Materials*. 2017; 154: 219-228. doi: 10.1016/j.conbuildmat.2017.07.178.
- Meddah M S, Lmbachiya M C, Dhir R K. Potential use of binary and composite limestone cements in concrete production. *Construction and Building Materials*. 2014; 58: 193-205. doi: 10.1016/j.conbuildmat.2013.12.012.
- Lee H-S, Wang X-Y. Hydration Model and Evaluation of the Properties of Calcined Hwangtoh Binary Blends. *International Journal of Concrete Structures and Materials*. 2021; 15. doi: 10.1186/s40069-020-00438-5.
- Bentz D P. Modeling the influence of limestone filler on cement hydration using CEMHYD3D. *Cement and Concrete Composites*. 2006; 28: 124-129. doi: 10.1016/j.cemconcomp.2005.10.006.
- Ylmén R, Jäglid U, Steenari B-M, Panas I. Early hydration and setting of Portland cement monitored by IR, SEM and Vicat techniques. *Cement and Concrete Research*. 2009; 39: 433-439. doi:10.1016/j.cemconres.2009.01.017.
- Mollah M Y, Kesmez M, Cocks D L. An X-ray diffraction (XRD) and Fourier transform infrared spectroscopic (FT-IR) investigation of the long-term effect on the solidification/stabilization (S/S) of arsenic(V) in Portland cement type-V. *Sci Total Environ*. 2004; 325:255-262. doi: 10.1016/j.scitotenv.2003.09.012.
- Trezza M, Lavat A J C, Research C. Analysis of the system $3\text{CaO} \cdot \text{Al}_2\text{O}_3 - \text{CaSO}_4 \cdot 2\text{H}_2\text{O} - \text{CaCO}_3 - \text{H}_2\text{O}$ by FT-IR spectroscopy. 2001; 31: 869-872.
- Lin R-S, Lee H-S, Han Y, Wang X-Y. Experimental studies on hydration–strength–durability of limestone-cement-calcined Hwangtoh clay ternary composite. *Construction and Building Materials*. 2021; 269: 121290. doi: 10.1016/j.conbuildmat.2020.121290.
- Li Q, Su A, Gao X. Preparation of durable magnesium oxysulfate cement with the incorporation of mineral admixtures and sequestration of carbon dioxide. *Sci Total Environ*. 2021; 809: 152127. doi: 10.1016/j.scitotenv.2021.152127.
- De Weerd K, Haha M B, Le Saout G, Kjellsen K O, Justnes H, Lothenbach B J C, et al. Hydration mechanisms of ternary Portland cements containing limestone powder and fly ash. 2011; 41: 279-291.
- Korea environment industry & technology institute, LCI DB emission factor. <http://www.epd.or.kr/eng/lci/lciCo200.do>, 2022 (accessed 10 March 2022).
- Zhang Y, Zhang J, Luo W, Wang J, Shi J, Zhuang H, et al. Effect of compressive strength and

chloride diffusion on life cycle CO₂ assessment of concrete containing supplementary cementitious materials. *Journal of Cleaner Production*. 2019; 218: 450-458. doi: 10.1016/j.jclepro.2019.01.335.

Campos H F, Klein N S, Marques Filho J, Bianchini M. Low-cement high-strength concrete with partial replacement of Portland cement with stone powder and silica fume designed by particle packing optimization. *Journal of Cleaner Production*. 2020; 261: 121228. doi: 10.1016/j.jclepro.2020.121228.

Yang K-H, Jung Y-B, Cho M-S, Tae S-H. Effect of supplementary cementitious materials on reduction of CO₂ emissions from concrete. *Journal of Cleaner Production*. 2015; 103: 774-783. doi: 10.1016/j.jclepro.2014.03.018.